Journal of Instrumentation

PAPER • **OPEN ACCESS**

Recent H^- ion source research and development at the Oak Ridge National Laboratory*

To cite this article: R.F. Welton *et al* 2023 *JINST* **18** C12011

Jinst

Published by IOP Publishing for Sissa Medialab

Received: *January 31, 2023*
Accepted: *October 9, 2023*
Published: *December 15, 2023*

8th International Symposium on Negative Ions, Beams and Sources
Orto Botanico, Padova, Italy
2–7 October 2022

Recent H^- ion source research and development at the Oak Ridge National Laboratory[1]

R.F. Welton,[a,*] B.X. Han,[a] M.P. Stockli,[a] S.N. Murray,[a] T.R. Pennisi,[a] C. Stinson,[a] V. Andzulis,[a] G. Terszakowec,[a] C. Piller,[a] O. Tarvainen[b] and D. Willis[a]

[a] *Spallation Neutron Source, Oak Ridge National Laboratory, Oak Ridge, TN 37831, U.S.A.*
[b] *STFC ISIS Pulsed Spallation Neutron and Muon Facility, Rutherford Appleton Laboratory, Harwell, U.K.*

E-mail: welton@ornl.gov

Abstract: The U.S. Spallation Neutron Source (SNS) is a state-of-the-art neutron scattering facility delivering the world's most intense pulsed neutron beams to a wide array of instruments which are used to conduct investigations in many fields of science and engineering. Neutrons are produced from spallation of liquid Hg by bombardment of short (~1 μs), intense (~35 A) pulses of protons delivered at 60 Hz by a storage ring which is fed by a high-intensity, ~1 GeV H^- LINAC. This facility has operated almost continuously since 2006, with ion source performance increasing over those years, and currently providing 50–60 mA of H^- ions with a duty-factor of 6% for maintenance-free runs of several months with near 100% availability. Ion source research and development at ORNL has played a key role in enabling and supporting this success: this report provides an update on some of the ongoing ion source research and development efforts which have been undertaken since the previous Negative Ion Beams and Sources (NIBS) conference in 2020. These include significant improvements to H^- beam current by extraction from a larger source outlet aperture and improvements to the electron dumping system which should eliminate the gradual loss of electrode voltage over the course of a run which has occasionally impacted SNS operations. Improvement and simplification of the plasma ignition system for the external antenna ion source, a long-standing problem, was also realized. Lastly, RF coupling efficiency was measured for both the SNS internal and external antenna ion sources.

Keywords: Accelerator Applications; Accelerator Subsystems and Technologies; Instrumentation for neutron sources; Ion sources (positive ions, negative ions, electron cyclotron resonance (ECR), electron beam (EBIS))

[1]This manuscript has been authored by UT-Battelle, LLC, under contract DE-AC05-00OR22725 with the US Department of Energy (DOE). This research was supported by the DOE Office of Science, Basic Energy Science, Scientific User Facilities. The US government retains and the publisher, by accepting the article for publication, acknowledges that the US government retains a nonexclusive, paid-up, irrevocable, worldwide license to publish or reproduce the published form of this manuscript, or allow others to do so, for US government purposes. DOE will provide public access to these results of federally sponsored research in accordance with the DOE Public Access Plan (http://energy.gov/downloads/doe-public-access-plan).

[*]Corresponding author.

https://doi.org/10.1088/1748-0221/18/12/C12011

Contents

2023 JINST 18 C12011

1 Introduction

The Spallation Neutron Source (SNS) is the highest-power pulsed neutron source currently operating worldwide and typically hosts ~1000 researchers per year. The SNS accelerator system is sequentially comprised of an H^- ion source, an electrostatic Low Energy Beam Transport (LEBT), a 2.5 MeV Radio Frequency Quadrupole accelerator (RFQ), a series of room-temperature linear accelerators followed by a series of superconducting RF cavities producing a ~1 GeV beam that is injected into a proton accumulator ring. The accumulated beam within the ring is then directed onto a liquid Hg target, producing neutrons [1]. The ion source produces pulses of H^- ions [2] now with a current of 50–60 mA, a pulse length of ~1 ms, and a repetition rate of 60 Hz [3]. A LEBT chopping system divides the ion source pulse into ~1000 mini pulses for beam stacking into the ring and a fast kicker magnet then directs the stacked beam (~35 A at 1 GeV, ~1 μs in duration) onto the Hg target with a repetition rate of 60 Hz. Currently, the SNS operates at 1.4 MW of proton beam power on target with plans to eventually reach 2.8 MW to simultaneously support a second target station (STS) [4]. Approximately 35 and 48 mA, measured at the exit of the RFQ, are needed to achieve the current and future target power requirements, respectively. The upgrade will also raise the accelerated beam energy from 1 to 1.3 GeV and increasing the extracted beam current from the source will ensure sufficient beam current at the exit of the RFQ. The SNS ion source now operates for service periods of up to ~4 months with a reliability of >99.5% using an internal antenna source [3, 5, 6].

This level of performance has come as a result of years of ion source research and development which has focused on continuous improvement of the SNS ion source, antennas, LEBT and supporting infrastructure [3, 5–8]. Today, the ion source R&D program is also focused on increasing the margin of available beam current for future facility upgrade projects like the second target station. These projects will require LEBT beam currents near the upper limit of its historical operating range and a healthy RFQ and will therefore greatly benefit from increased output from the ion source within the acceptance of the RFQ. See, for example ref. [7]. A secondary goal of the program is to develop the

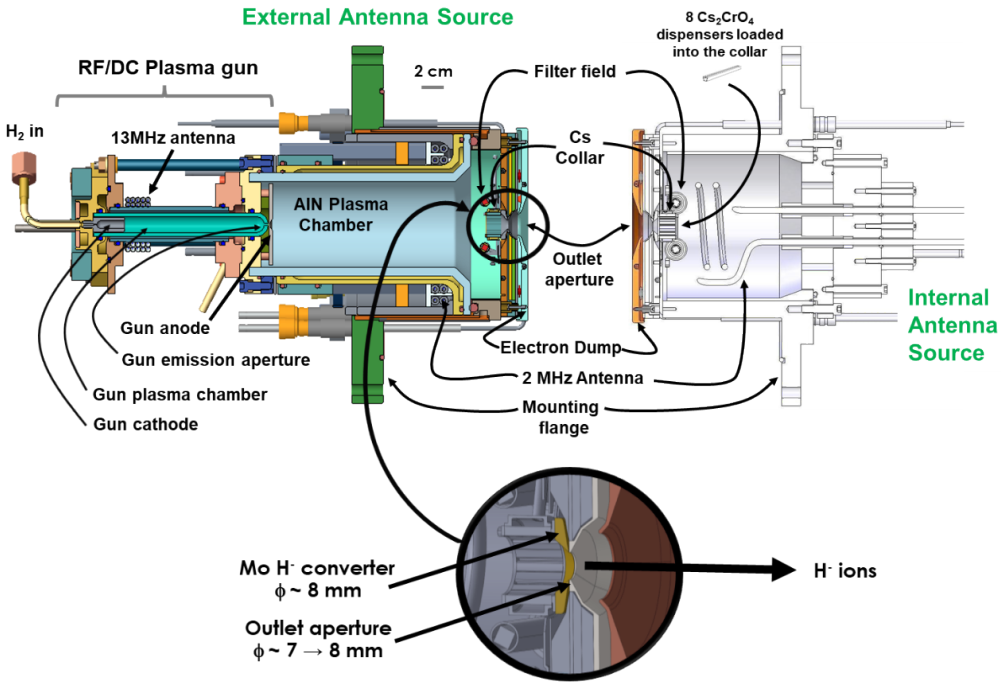

Figure 1. Schematic cross-section of the SNS internal (right) and external antenna (left) ion source with corresponding major components labeled. The inset (below) shows a detailed view of the source outlet aperture and H^- converter which is the same for both sources.

SNS external antenna source which will eliminate the small risk of using internal antennas which are fabricated by a single vender using a proprietary process. Specifically, efforts are currently being directed towards improving plasma ignition for this source which is more challenging due to the external location of the antenna [7]. This report will detail some of our successful R&D efforts since the last NIBS which include tests with a larger extraction aperture, improved plasma ignition in the external antenna source, RF coupling efficiency measurements and improved electron dumping.

2 The SNS ion sources

Figure 1 shows the SNS internal and external antenna ion sources which have been described previously [2, 3, 5]. Both are Cs-enhanced, RF-driven, multicusp ion sources, fed by a pulsed 2 MHz RF generator (1 ms, 60 Hz) providing ~50 kW of RF power to a helical antenna which forms a high-density plasma within the discharge chamber. The plasma formed by inductive coupling feeds a smaller low-temperature plasma region of the source. This low-temperature region is bounded radially by a Cs collar ($\phi \sim 1.9$ cm) and it extends axially to the source outlet aperture ($\phi = 7$ mm) and upstream to a transverse ~250 G magnetic filter field that divides each plasma region. Those H^- ions formed mostly in the low-temperature region, either on the surface or within the plasma volume, can diffuse through the outlet aperture and are then accelerated into a beam by a ~6 kV biased electron dump electrode (see figure 1) and subsequently to 65 kV as the beam enters the LEBT passing through a grounded extraction electrode. Electrons which are extracted along with the negative ions are deflected out of the beam path by a ~1600 G transverse magnetic field and mostly

2023 JINST 18 C12011

strike the electron dump electrode, although some travel into the LEBT and are dumped onto a water-cooled electron target. Currently, the SNS uses one of 3 internal antenna ion sources for neutron production (same design) as well as 3 research internal and 3 external antenna ion sources used on the SNS test facilities. The outlet aperture assemblies (components downstream of the antenna) are nearly identical and easily interchangeable between all internal and external antenna sources. These sources differ in that the SNS internal antenna source employs a porcelain-enamel-coated Cu 2.5-turn antenna immersed within the plasma chamber itself while the external antenna source employs a ~7 mm thick AlN plasma chamber surrounded by a 3.5-turn Cu antenna. The internal antennas are coated with a proprietary porcelain mixture to a thickness of ~0.5 mm by a local vender [9]. The sources also employ different plasma ignition systems: the internal antenna utilizes ~300 W of continuously applied RF power (13.56 MHz) to create a continuous low-density discharge which serves to quickly ignite the high-density plasma when pulsed 2 MHz power applied to the same antenna. The external antenna source utilizes a plasma gun which continuously injects electrons into the main plasma chamber facilitating ignition during the 2 MHz RF pulse. High-density plasma ignition is more difficult in the external antenna source like due to the greater distance between the antenna and plasma which results in reduced RF field strength and lower capacitive coupling.

3 Recent R&D efforts: exploring larger outlet apertures

In 2012 we studied variations in H^- converter aperture diameters (see figure 1 inset) and found that larger ones seemed to contribute to increased H^- beam current from the ion source [8]. Since then, we standardized this structure to have $\phi \sim 8.2$ mm (design = 7 mm) diameter apertures in our production ion sources. At that time, we left the source outlet aperture diameter fixed ~7 mm. This year, due to the desire for higher beam current margins, we reconsidered increasing the source outlet aperture diameter by ~1 mm [10]. The approach of increasing the source outlet aperture diameter was under consideration for some time at the SNS and was motivated by the following factors: (i) potentially increasing beam current due to having a ~30% larger plasma emission surface, (ii) H_2 flow out of source is restricted by conductance through 2 apertures and a cylindrical Cs collar. Vacuum calculations suggest that only a modest flow increase will be needed to maintain equal pressure in the source. (iii) Manageable increase of beam emittance with higher currents compared to the RFQ acceptance: experience at J-PARC and beam simulations (see below) suggest emittance growth should not significantly impact beam accepted into the RFQ.

Figure 2 shows PBGUNS simulations for beam extracted from the source and transported through the electrostatic LEBT [11]. The simulation, shown in figure 2a, was performed using the $\phi \sim 7$ mm source outlet aperture under nominal conditions. Simulations were then run under the same conditions except with a larger $\phi \sim 8$ mm source outlet aperture as shown in figure 2b. Injected current density and plasma parameters were set to match our experimentally observed beam current and emittance for the nominal 7 mm source outlet aperture and held constant during the simulation of the enlarged outlet aperture. Figure 3 shows the transverse emittance produced by the simulation in the entrance plane to the RFQ as well as the approximate RFQ acceptance represented as a simple ellipse. These plots show that similar fractions of the transportable beam current are within the acceptance for both source outlet aperture sizes suggesting similar compatibility with the RFQ.

2023 JINST 18 C12011

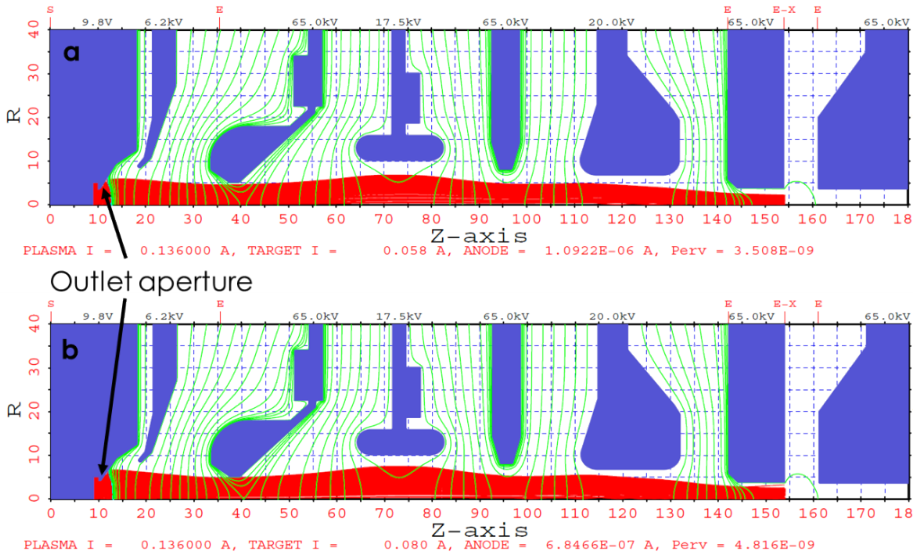

Figure 2. PBGUNS beam profile simulations for beam extracted from the source and transported through the LEBT for source for (a) nominal ϕ = 7 mm source outlet aperture and (b) enlarged ϕ = 8 mm source outlet aperture with the same electrode potentials.

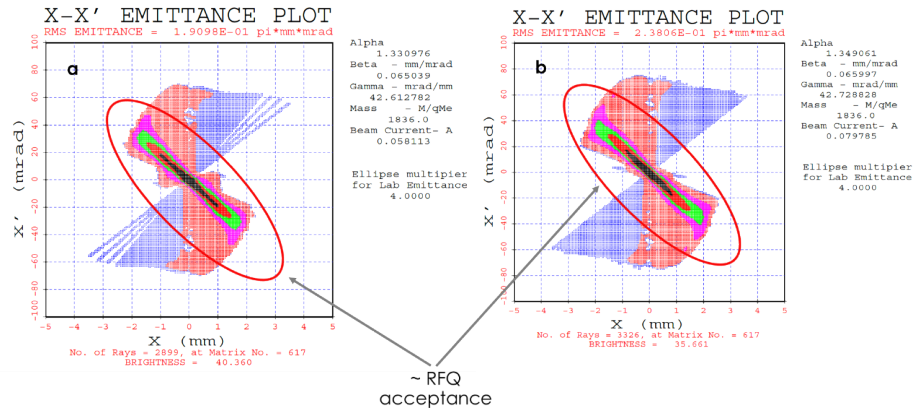

Figure 3. PBGUNS transverse emittance plots at the RFQ entrance (z = 154 mm) for (a) the nominal ϕ = 7 mm aperture and (b) the enlarged ϕ = 8 mm aperture.

Figure 4 shows a plot of the multiday measured beam current extracted from a SNS production ion source with an internal antenna during initial tests on the Ion Source Test Facility (ISTS) [12]. The source was first equipped with a ϕ = 7.2 mm (figure 4a) and then with a ϕ = 8.2 mm (figure 4b) source outlet aperture and measurements were made using a faraday cup and a toroidal beam current monitor located at the exit of the LEBT. The data show that 25–30% more beam current (53 $\rightarrow$ 67 mA) could be extracted. In both cases, the source could be operated stably by feeding H_2 gas at the rate of 30–40 SCCM into the source. As evident from the figure, the smaller aperture operated toward the lower end of this range while the larger aperture seemed to require higher flows toward the upper end of the range. RF power of ~55 kW and acceleration voltage of ~65 kV was held constant over these measurements. Initial emittance measurements are being performed and will be presented in a later article.

2023 JINST 18 C12011

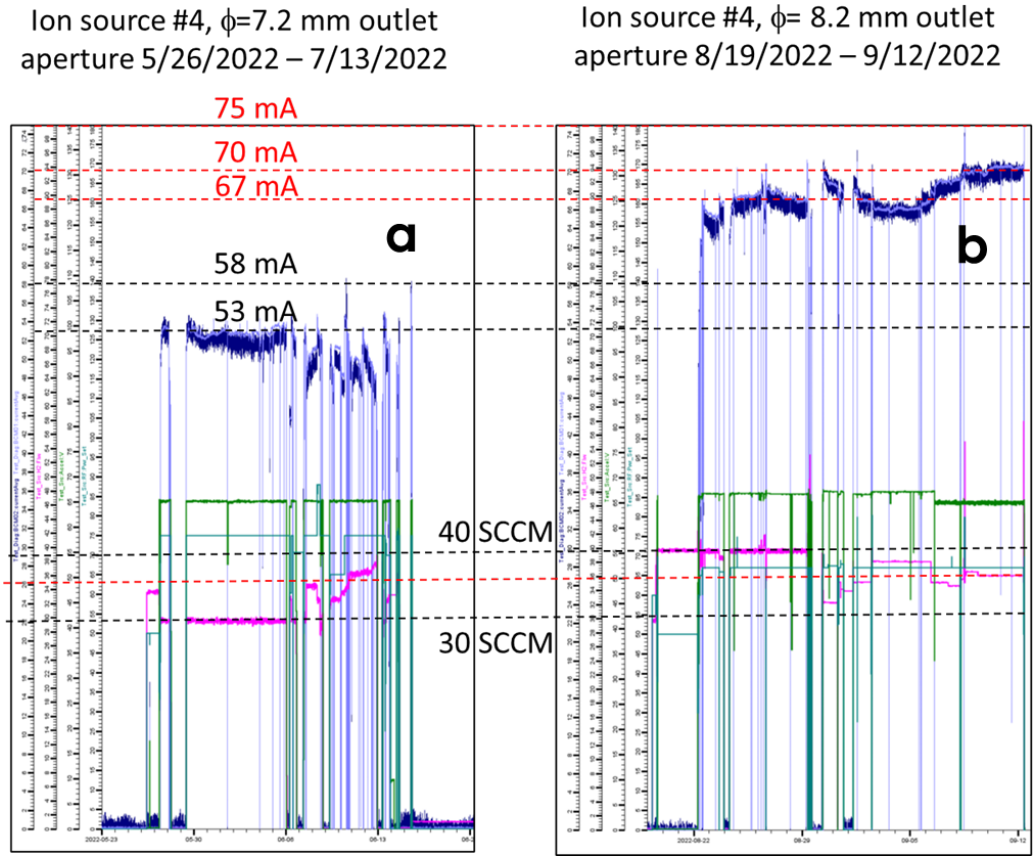

Figure 4. Beam current measured from a SNS production, internal antenna ion source measured at the exit of the LEBT using a (a) ϕ = 7.2 mm and (b) ϕ = 8.2 mm source outlet aperture. The measurements were performed on the ISTS. RF power ~55 kW and acceleration voltage of ~65 kV were held constant.

4 Improving plasma ignition in the external antenna source

In recent years, R&D efforts related to the external antenna ion source was reduced in priority due to reliable operation of the internal antenna on the SNS accelerator and having acquired a large inventory of top-tier antennas (last failure on the SNS accelerator was ~9 years ago) [12].

Recently, however, 2 second-tier internal antenna failures have occurred on source #4 at the ISTS (7-11-22) and BTF (3-19-22) reminded us of the importance of having a contingency ion source for the SNS. Previously, extensive long-term testing of the external antenna source on the BTF during 2016–2020 revealed that reliable ignition of the plasma, over a run-period of several months, was problematic due to inconsistent performance of the RF/DC plasma ignition gun over time [7]. This gun is pictured to the left in figure 1 and, as mentioned earlier, is required for reliable ignition of the main 2 MHz plasma. To address this, a dedicated plasma gun test bench was constructed which allows study and optimization of the gun itself. The bench consists of a vacuum chamber, pumped by a 700 l/s turbo molecular pump, with flanges allowing the plasma gun to be directly mounted. The gun can then be operated normally with output measured directly by a current collection probe which could be positioned at various distances from the emission aperture of the gun. The bench also houses DC (3 kV, 33 mA), pulsed (4 kV, 20 mA) and RF (13 MHz, 600 W) power supplies as

2023 JINST 18 C12011

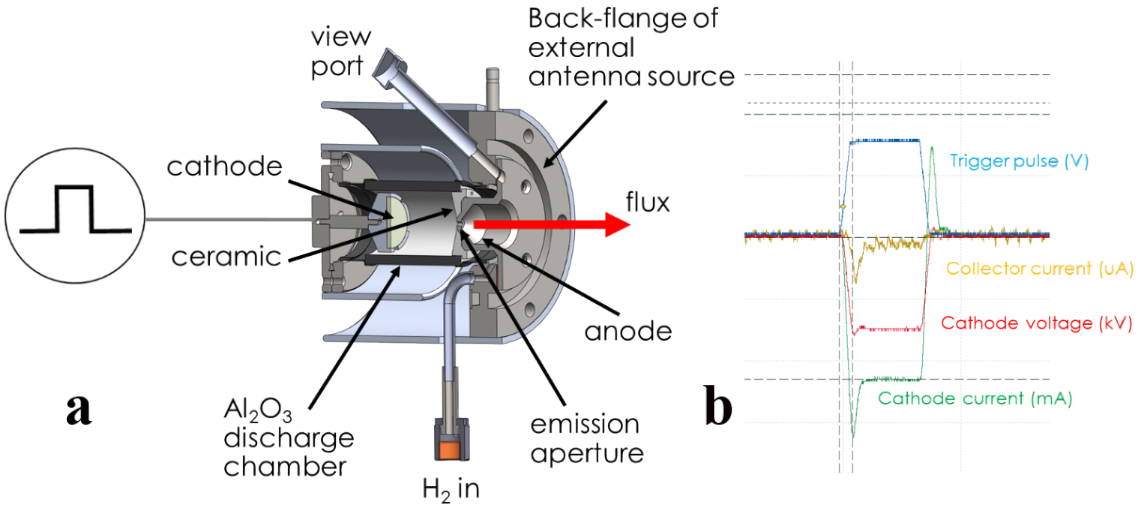

Figure 5. (a) Cross sectional view of the new pulsed plasma gun which affixes to the rear of the external antenna source shown in figure 1. (b) Typical voltage and current pulse shapes recorded with the Pico scope during gun operation on the test bench for reference. Units are arbitrary with numerical values given in figure 6.

well as a Pico scope and signal generator which were used to explore various configurations and operational modes of the gun.

During experimentation with the RF/DC gun shown in figure 1 it became clear that lengthening the W gun cathode, thereby reducing the cathode-anode gap to 3.5 cm and applying pulsed voltage (1–4 kV) to the cathode eliminated the need for the 13 MHz RF antenna/power supply and resulted in very stable plasma operation of the gun delivering comparable current to the collection probe. In fact, when the gun was operated in this mode (0.5 ms, 60 Hz, 2600 V) a stable discharge was achieved with ~6 mA of discharge current and ~1 mA collected on the probe located a few mm from the emission aperture (ϕ = 2 mm) of the gun. This prototype configuration was then run unattended on the test bench for ~4 months holding these parameters. Next, this gun was refurbished and attached to an external antenna ion source where it ignited the source reliably for ~2 months on the ISTS (1 ms, 3000 V, 6 mA, 60 Hz) with no loss of discharge current. These initial results, along with the improved simplicity of eliminating the 13 MHz system, motivated us to design, build and test an optimal pulsed-DC production quality plasma ignition gun.

Figure 5a shows the new pulsed plasma gun which mounts to the rear of the external antenna source in place of the RF/DC plasma gun shown in figure 1. The more efficient nature of the pulsed discharge (<1 W of dissipated power versus several hundred watts in the RF gun) allows the design to be greatly simplified: eliminating the need for water cooling and the consequent elimination of the internal o-rings. The gun discharge chamber utilizes an off-the-shelf Al_2O_3 break and a W cathode and anode which features a ϕ = 2 mm emission aperture as used in the earlier RF/DC plasma guns. An additional ceramic was also added over the anode to improve gun efficiency using the hollow anode effect [13]. The anode-cathode gap was determined by the minimum of the Paschen breakdown curve for the measured and calculated chamber pressure at the operating H_2 feed-rate of the ion source as all source gas flows through the gun. The gas and power efficiency of the gun were

2023 JINST 18 C12011

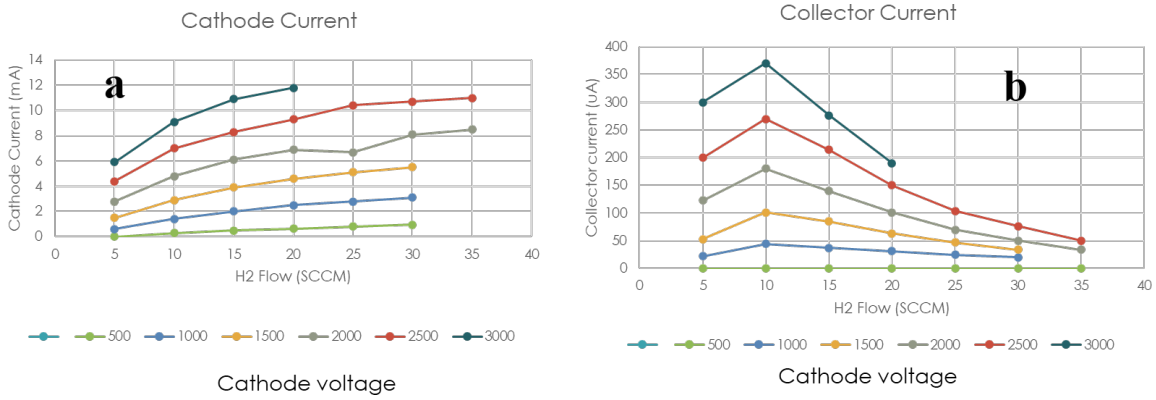

Figure 6. (a) Cathode (discharge) current drawn from the Trek power supply as a function of H2 flow into the gun and voltage of the power supply. (b) Collector current from the probe located ~3.5 cm from the emission aperture. Straight lines connecting actual data points assist in visualization.

maximized by using electrostatic simulation software to ensure the electric field is uniform across the discharge volume thereby eliminating regions of weak electric field which could choke the discharge (<300 V/cm) [14]. The design also features gaseous H_2 injection at source potential eliminating the need for a dedicated HV break in the feedline as required in all earlier gun designs [7]. In addition, the entire gun assembly shown in figure 5 is bakeable to ~400 C.

Testing of the new pulsed plasma gun has begun on the test bench utilizing cathode voltage pulses of width 0.5 ms and repetition rate of 60 Hz. Upon initial startup, the gun immediately operated at the current limit of the power supply and therefore required a series limiting resistor to stabilize the discharge. This was expected from the Paschen theory of glow discharges [14]. A 150 kΩ resistor was used to allow the gun to operate within the current limits of the pulsed power supply. Figure 5b shows typical cathode and collector current and voltage pulse shapes measured by the Pico scope in arbitrary units. The actual measured cathode and collector current values as a function of H_2 feed-rate (5–35 SCCM) and cathode voltage (0.5–3 kV) are plotted in figure 6. Cathode current and voltage were measured from a monitor port on the pulsed power supply and the collector current was measured using an unbiased movable probe located ~3.5 cm from the emission aperture of the gun. It should be noted that due to geometrical constraints the collection probe could not be positioned as close to the emission aperture as in earlier measurements of the prototype gun. Note that the plotted cathode voltage and current are read from the power supply and do not account for the voltage drop through the series resistor.

These preliminary tests demonstrate that the pulsed plasma gun, shown in figure 5, can be operated reliably over a wide range of H_2 flow-rates and pulsed cathode voltages, igniting without issue and emitting stable pulses of charged plasma particles. Power efficiency and available discharge current greatly exceed earlier versions of the plasma ignition guns used with the SNS external antenna source. Since optimum emission was found at ~10 SCCM, about 1/3 of the nominal H_2 flow-rate for the ion source, future experiments will explore larger gun emission apertures. This should significantly increase the emitted charged particle flux by allowing the gun to operate at optimal pressure and benefit from increased emission area. The next steps, with regard to the development of plasma gun, will be to (i) test with a larger aperture, (ii) modify the current collection probe to allow close proximity to the emission aperture and (iii) test with an external antenna source on the ISTS.

2023 JINST 18 C12011

Another area of R&D effort since the last NIBS was to explore an alternative approach to plasma ignition in the external antenna ion source: eliminating the plasma gun altogether and directly feeding continuous, low-level, 13 MHz into the main 2 MHz antenna (see figure 1) as is routinely done with the operational SNS internal antenna source. This was tried in earlier years on the external antenna source without success. In recent experiments, circuit analysis software was used to modify the 13 MHz matching network to accommodate the higher inductance of the external antenna. Next, a Butterworth filter was added to the output of the 13 MHz generator to protect it from the high 2 MHz power. During testing the resonance tune of matching network was found to be sharply peaked and required the use of a network analyzer to set the initial positions of the tuning capacitors. This configuration was then tested for several weeks on the ISTS in January 2022 and ran stably but required ~500 W of 13 MHz power (nominal is ~300 W for the internal antenna source) and ~33–40 SCCM of H_2 gas flow (nominal is ~30 SCCM). We will continue to explore this option but, at this time, the simplicity and dramatically higher power efficiency of the pulsed plasma gun seems more attractive and more likely to support lower H_2 flows which will benefit the overall H^- ion source performance. Some external antenna RF-sources used in other facilities also employ the plasma gun approach to ignition [10, 15, 16].

5 2 MHz RF coupling efficiency measurements

In collaboration with RAL-ISIS [17] and following the methodology of Zielke [18] we conducted RF coupling efficiency measurements with both the SNS internal and external ion sources. These measurements were made to support modelling efforts which require the total RF power absorbed by the plasma (i.e. power not lost to the RF structures) and are not directly related to ion creation efficiency. Let η be the RF coupling efficiency and P_p be the power absorbed by the plasma and P_g be the net power delivered from the generator to the RF circuit as measured by a directional coupler (i.e. forward power-reflected power). Let P_{loss} be the power lost to the transmission line, transformer, matching circuit, RF antenna and ohmic heating of surrounding metal structures, etc. Then,

$$\eta = \frac{P_p}{P_g} = \frac{P_g - P_{\text{loss}}}{P_g} \quad \text{where} \quad P_{\text{loss}} = \frac{1}{2} R_{\text{net}} I_0^2.$$

These losses can be quantified by an effective network resistance R_{net} with I_0 being the measured RMS current circulating through the antenna and matching network as measured by a commercial current transformer installed between the antenna and matching network. The experiment was conducted on both internal and external antenna sources by scanning RF power from approximately 1 to 20 kW first with no plasma (no H_2 gas flow) while recording antenna current and P_g with the matching network tuned for normal plasma operation. Since no plasma is being generated all the transferred power from the generator is dissipated by the structure and therefore $P_{loss} = P_g$. Plotting the measured P_g versus $\frac{1}{2} I_0^2$ reveals an essentially linear curve for both sources allowing determination of the $R_{net} = 0.36\,\Omega$ for the internal antenna source and 0.58 Ω for the external antenna source. Next, P_g is determined with the source plasma lit as a function of I_0 as power is increased to operational levels. The above equation can then be solved for the RF coupling efficiency η for each source at nominal power level and was found to be η = 55–60% for the external antenna source and η = 75–77% for the internal antenna source [17, 18]. This can help explain why it is more difficult to implement two-frequency excitation in an external versus an internal antenna source.

2023 JINST 18 C12011

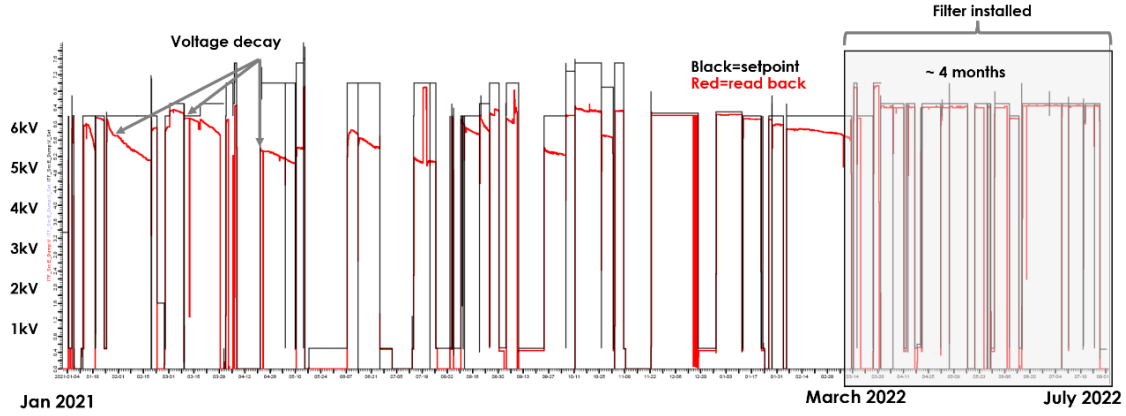

Figure 7. Archived electron dump power supply voltage record spanning ~1.5 years of ion source operation on the BTF. Voltage decay over time is observed until the circuit was installed in March 2022.

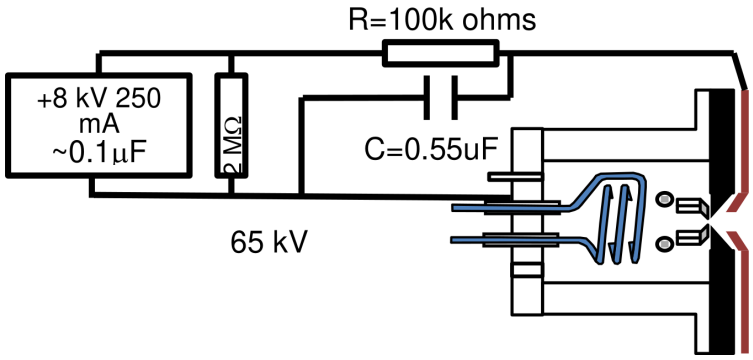

Figure 8. Electron dump power supply isolation circuit used to stabilize the electron dump electrode voltage.

6 Improving the stability of the electron dump voltage

The final topic of the R&D efforts discussed here is related to improving a long-standing problem of the electron dumping electrode voltage (+6.2 kV continuous) gradually sagging over the course of long run periods on the SNS accelerator and test stands. For example, figure 7 shows this phenomenon on the BTF during source operation from Jan 2021 to March 2022. At the beginning of each H^- pulse (during plasma ignition), electron spikes of several hundred mA are extracted from the source plasma [19]. These current spikes of several hundred mA likely increase over the course of a run (as Cs depletes) thereby encroaching on the 250 mA current limit of the power supply. Current draw during and between RF pulses outside of these spikes are observed to be well within the limit of the power supply during the entire run-period. To address this, the RC circuit shown in figure 8 was added to the output of the power supply. This is similar to circuits tried at the SNS in the past [19]. In general, during the current spike, this circuit will reduce the current drawn from the power supply by a factor of $\Delta t/RC$, where Δt is the width of the electron current spike, by sourcing this current from an external capacitor rather than directly from the power supply. This greatly increases the pulsed current limit of the power supply. The configuration was installed on the BTF in March 2022 and so far eliminated the gradual voltage decay over time as can be seen in figure 7.

2023 JINST 18 C12011

Similar success was achieved on the ISTS for over 4 months of operation and, in the future, we will likely implement a version this circuit on the SNS accelerator after extensively testing on the BTF and ISTS.

References

[1] S. Henderson, *The Spallation Neutron Source accelerator system design*, *Nucl. Instrum. Meth. A* **763** (2014) 610.

[2] R. Keller et al., *Design, Operational Experiences and Beam Results Obtained with the SNS H^- Ion Source and LEBT at Berkeley Lab*, *AIP Conf. Proc.* **639** (2002) 47.

[3] B. Han et al., *Recent performance of the SNS H^- ion source with a record long run*, *AIP Conf. Proc.* **2373** (2021) 040004.

[4] J. Galambos, *Final Design Report Proton Power Upgrade*, ORNL report, ORNL/TM2020/1570-R0 (2020).

[5] M.P. Stockli, R.F. Welton and B. Han, *Record productions establish RF-driven sources as the standard for generating high-duty-factor, high-current H^- beams for accelerators (Winner of the ICIS 2017 Brightness Award)*, *Rev. Sci. Instrum.* **89** (2018) 052202.

[6] R.F. Welton et al., *Installation and commissioning of the ion source systems for the new spallation neutron source 2.5 MeV injector*, *Rev. Sci. Instrum.* **91** (2020) 013334.

[7] R.F. Welton et al., *H^- Ion Source Research and Development at the Oak Ridge National Laboratory*, *AIP Conf. Proc.* **2373** (2021) 070004.

[8] R.F. Welton et al., *Developing reliable internal antennas and standardizing performance of H^- RF ion sources*, *AIP Conf. Proc.* **1515** (2013) 341.

[9] Cherokee Porcelain Enamel Corporation, 2717 Independence Lane, Knoxville, TN 37914, U.S.A.

[10] R. Welton et al., *Negative hydrogen ion sources for particle accelerators: Sustainability issues and recent improvements in long-term operations*, *J. Phys. Conf. Ser.* **2244** (2022) 012045.

[11] https://www.far-tech.com.

[12] R.F. Welton et al., *Improvements to the internal and external antenna H^- ion sources at the Spallation Neutron Source*, *Rev. Sci. Instrum.* **85** (2014) 02B135.

[13] A. Anders and S. Anders, *The working principle of the hollow-anode plasma source*, *Plasma Sources Sci. Technol.* **4** (1995) 571.

[14] J.R. Roth, *Industrial Plasma Engineering*, IOP Publishing, Bristol, U.K. (1995).

[15] J. Peters, *The Status of DESY H^- Ion Sources*, in the proceedings of the *XX International Linac Conference*, Monterey, CA, U.S.A. (2000), p. MOD06.

[16] W. Chen et al., *Operation of RF-driven negative hydrogen ion source in CSNS*, *Rev. Sci. Instrum.* **90** (2019) 113320.

[17] S. Lawrie et al., *RF efficiency measurements of inductively-coupled plasma H^- ion sources at accelerator facilities*, *J. Phys. D* **56** (2023) 085202.

[18] D. Zielke, S. Briefi and U. Fantz, *RF power transfer efficiency and plasma parameters of low pressure high power ICPs*, *J. Phys. D* **54** (2021) 155202.

[19] M.P. Stockli, *Recent performance and ignition tests of the SNS H^- ion source for 1-MW neutron production*, *AIP Conf. Proc.* **1655** (2013) 030001.

2023 JINST 18 C12011